materials

Article

Critical Current Density and Meissner Effect of Smart Meta-Superconductor MgB_2 and Bi(Pb)SrCaCuO

Honggang Chen, Yongbo Li, Yao Qi, Mingzhong Wang, Hongyan Zou and Xiaopeng Zhao *

Smart Materials Laboratory, Department of Applied Physics, Northwestern Polytechnical University, Xi'an 710129, China; 2017100698@mail.nwpu.edu.cn (H.C.); 2014100616@mail.nwpu.edu.cn (Y.L.); qiyao@mail.nwpu.edu.cn (Y.Q.); wangmingzhongsuper@163.com (M.W.); 2019202522@mail.nwpu.edu.cn (H.Z.)
* Correspondence: xpzhao@nwpu.edu.cn

Abstract: The smart meta-superconductor MgB_2 and Bi(Pb)SrCaCuO increase the superconducting transition temperature (T_C), but the changes in the transport critical current density (J_C) and Meissner effect are still unknown. Here, we investigated the J_C and Meissner effect of smart meta-superconductor MgB_2 and Bi(Pb)SrCaCuO. The use of the standard four-probe method shows that Y_2O_3:Eu^{3+} and Y_2O_3:Eu^{3+}+Ag inhomogeneous phase significantly increase the J_C, and J_C decreases to a minimum value at a higher temperature. The Meissner effect was measured by direct current magnetization. The doping of Y_2O_3:Eu^{3+} and Y_2O_3:Eu^{3+}+Ag luminescent inhomogeneous phase causes a Meissner effect of MgB_2 and Bi(Pb)SrCaCuO at a higher temperature, while the non-luminescent dopant reduces the temperature at which samples have Meissner effect. The introduction of luminescent inhomogeneous phase in conventional MgB_2 and copper oxide high-temperature Bi(Pb)SrCaCuO superconductor increases the T_C and J_C, and Meissner effect is exerted at higher temperature. Therefore, smart meta-superconductivity is suitable for conventional and copper oxide high-temperature superconductors.

Keywords: smart meta-superconductor; transport critical current density; Meissner effect; critical transition temperature

check for updates

Citation: Chen, H.; Li, Y.; Qi, Y.; Wang, M.; Zou, H.; Zhao, X. Critical Current Density and Meissner Effect of Smart Meta-Superconductor MgB_2 and Bi(Pb)SrCaCuO. *Materials* **2022**, *15*, 972. https://doi.org/10.3390/ma15030972

Academic Editor: Yong Seung Kwon

Received: 29 November 2021
Accepted: 25 January 2022
Published: 27 January 2022

1. Introduction

Superconductivity has greatly expanded people's understanding of condensed matter physics and greatly promoted the progress of industrial technology [1,2]. In the superconducting state, superconductors have zero-resistance characteristic and complete diamagnetism (Meissner effect) [3–7]. The zero-resistance characteristic and Meissner effect are both independent and closely related to each other. A material must satisfy the zero-resistance characteristic and the Meissner effect simultaneously to determine whether it is a superconductor [2].

All superconductors transition from a superconducting state to a non-superconducting state may have their own characteristic parameters: critical transition temperature (T_C), critical current density (J_C), and critical magnetic field (H_C) [1,3]. Critical current density J_C is an important parameter to characterize superconductivity, and it is also one of the main parameters to measure the performance of superconducting materials in engineering technology applications. In scientific research, the electric transport and hysteresis loop methods are two widely used methods to measure the critical current [8]. The electric transport method is accurate and reliable, and it is used in the international critical current measurement standard. Electrical transport measurement usually uses the four-probe method. After a certain current I is input into the sample through the current lead, the voltage V of the sample is measured. The critical current I_C is defined as the transport current when a significant drift voltage exists [9–11]. The current–voltage (I–V) curve is used to determine the critical current I_C, which then enables the determination of the critical current density J_C [12,13].

Since the discovery of superconductivity, increasing transition temperature and transport critical current density of the superconductor has been the main research direction of superconductivity. At present, the commonly used methods to increase the superconducting transition temperature are to modify existing superconductors and develop new superconducting materials, such as doping Al [14], C [15], and Li [16] in MgB_2 and doping Cs [17], SnO_2 [18], and ZrO_2 [19] in a BiSrCaCuO superconductor. However, the dopants are unstable at a high temperature and will react with the superconductor. Thus, this method cannot increase the superconducting transition temperature. In recent years, researchers have found that hydrides have a higher transition temperature under high pressure. For example, a superconductivity of 203 K was observed in a sulfur hydride system at 155 GPa [20], superconductivity of 250 K in LaH_{10} at 170 GPa [21], and the room temperature superconductivity of 287.7 K in a carbonaceous sulfur hydride system at 267 GPa [22]. Although this approach can achieve a higher superconducting transition temperature and even room-temperature superconductivity, the extremely high pressure and small sample size limits its further applications. Thus far, there is no particularly good strategy for increasing the superconducting transition temperature. Chemical doping is the easiest way to change the J_C of superconductor because it does not require costly raw materials or complex technologies. For example, doping graphene [23] and Dy_2O_3 [24] in MgB_2 and doping Al_2O_3 [25], MgO [26], and SiC [27] in BiSrCaCuO decrease its J_C in self-field. Meanwhile, doping anthracene into MgB_2 [28] and doping Cr_2O_3 [29], SnO_2 [30], and ZnO [31] in BiSrCaCuO will increase its J_C in self-field. Although the J_C of superconductor increases or decreases in self-field due to chemical doping, the corresponding T_C decreases. Therefore, no particularly effective method can increase the T_C and J_C at the same time in self-field.

A metamaterial is a kind of composite material with an artificial structure. It exhibits supernormal physical properties that natural materials do not possess, and these supernormal properties are determined by special artificial structures [32,33]. Recently, Smolyaninov et al. proposed that a higher transition temperature can be obtained by constructing a metamaterial superconductor with an effective dielectric constant of nearly zero or hyperbolic metamaterial superconductor [34–36]. In 2007, our research group proposed to introduce an inorganic ZnO electroluminescence (EL) material in the high-temperature Bi(Pb)SrCaCuO superconductor to influence the Bi(Pb)SrCaCuO superconducting transition temperature [37–39]. Y_2O_3 is a non-electroluminescent material and can become a kind of electroluminescent material after the addition of a small amount of Eu^{3+} ions as the luminous center. Y_2O_3:Eu^{3+} is a rare earth luminescent material with excellent performance. In addition, the preparation of Y_2O_3:Eu^{3+} into Y_2O_3:Eu^{3+}+Ag topological luminophore can further improve its EL performance. With the development of a metamaterial, we constructed a MgB_2 and Bi(Pb)SrCaCuO smart meta-superconductor in recent years. The smart meta-superconductors are composed of superconducting particles and Y_2O_3:Eu^{3+} and Y_2O_3:Eu^{3+}+Ag luminescent inhomogeneous phases. We doped Y_2O_3:Eu^{3+} and Y_2O_3:Eu^{3+}+Ag EL materials in conventional MgB_2 and high-temperature Bi(Pb)SrCaCuO superconductors [37–44]. The research results showed that the doping of Y_2O_3:Eu^{3+} and Y_2O_3:Eu^{3+}+Ag EL materials increases the T_C of MgB_2 and Bi(Pb)SrCaCuO. The T_C of MgB_2 is increased by 1.2 K, and the zero resistance temperature $T_{C,0}$ and the onset transition temperature $T_{C,on}$ of Bi(Pb)SrCaCuO are increased by 4 and 6.3 K, respectively. We believe that this result is due to superconducting particles acting as microelectrodes to excite the EL of the luminescent inhomogeneous phases under the action of an external electric field. EL energy injection promotes the formation of electron pairs. Accordingly, the T_C of MgB_2 and Bi(Pb)SrCaCuO can be increased via EL [43,44].

In previous studies, the T_C of MgB_2 and Bi(Pb)SrCaCuO were increased by constructing a smart meta-superconductor. However, the J_C and Meissner effect were not studied. This study investigates the J_C and Meissner effect of MgB_2 and Bi(Pb)SrCaCuO smart meta-superconductor. The results show that the addition of Y_2O_3:Eu^{3+} and Y_2O_3:Eu^{3+}+Ag luminescent inhomogeneous phase increases the T_C of MgB_2 and Bi(Pb)SrCaCuO, while increasing the J_C and the J_C of the luminescent inhomogeneous phase doped samples decreases to a minimum value at higher temperatures. The direct current (DC) magnetization data indicate that Y_2O_3:Eu^{3+} and Y_2O_3:Eu^{3+}+Ag luminescent inhomogeneous phase doping causes a Meissner effect of MgB_2 and Bi(Pb)SrCaCuO at a higher temperature, while non-luminescent dopant doping reduces the temperature of the Meissner effect.

2. Experiment

2.1. Preparation and Characterization of Pure MgB_2 and Doping MgB_2 Superconducting Samples

Using MgB_2 with three different particle sizes, three series of samples doped with a luminescent inhomogeneous phase or non-luminescent dopant were prepared by ex-situ sintering, and the samples were marked as $^aMgB_2$ (Φ_a < 30 μm), $^bMgB_2$ (Φ_b < 15 μm), and $^cMgB_2$ (Φ_c < 5 μm) series samples, and the thickness of prepared bulk samples is 1.2 mm. X-ray diffraction (XRD) and scanning electron microscope (SEM) characterization show that the main phase of all samples is MgB_2, a small amount of MgO impurity phase is detected, and the particle sizes of $^aMgB_2$, $^bMgB_2$, and $^cMgB_2$ decrease sequentially. The curve of the temperature dependence of resistivity (*R*–*T*) shows that the non-luminescent dopants Y_2O_3 and Y_2O_3:Sm^{3+} doping decreases the T_C of MgB_2, while the luminescent inhomogeneous phase Y_2O_3:Eu^{3+} and Y_2O_3:Eu^{3+}+Ag doping increases the T_C of MgB_2 in different amplitudes. The preparation process and related characterization of pure MgB_2 and doped MgB_2 samples were described in [44].

2.2. Preparation and Characterization of Pure B(P)SCCO and Doping B(P)SCCO Superconducting Samples

Three series of pure B(P)SCCO and doped B(P)SCCO superconducting samples with different particle sizes were prepared using three kinds of B(P)SCCO raw materials with successively decreasing particle sizes, and the samples were marked as A (A1–A6), B (B1–B6), C (C1–C7) series samples. The thickness of prepared bulk samples is 1.2 mm. XRD and SEM show that the main phase of the prepared samples is the high-temperature phase Bi2223, which contains a small amount of the low-temperature phase Bi2212, and the microstructure is a randomly distributed plate-like structure. The particle sizes of A, B, and C series samples decrease in turn. *R*–*T* test indicates that the non-luminescent dopants Y_2O_3 and Y_2O_3:Sm^{3+} doping decreases the T_C of B(P)SCCO, while the T_C of B(P)SCCO increases with the doping of luminescent inhomogeneous phases Y_2O_3:Eu^{3+} and Y_2O_3:Eu^{3+}+Ag. The preparation process and related characterization of samples were described in [43,45].

2.3. Testing of Transport Critical Current Density and Meissner Effect

As usually conducted in superconducting systems, transport critical current density (J_C) was determined by *I*–*V* measurements at different temperatures (below the onset transition temperature $T_{C,on}$) with a voltage criterion of 1 μV/cm [8,12,13]. Subsequently, DC magnetization measurements were performed on the prepared samples [46]. The samples were cooled slowly in a magnetic field of 1.8 and 2.5 mT parallel to the plane, and data were collected during heating. All samples are fully diamagnetic.

3. Results and Discussion

As usually conducted in superconducting systems, *I*–*V* curves of superconductors at different temperatures were used to extract I_C. The *I*–*V* curves of the samples were tested by a four-probe method. A test current was applied to the prepared samples, and a Keithley digital nanovoltmeter was used to measure the high resolution voltage. Figure 1 shows the *I*–*V* curves of pure B(P)SCCO (A1) at different temperatures (106, 108, 110, and 112 K). The extraction criteria of I_C are given in this figure, and the I_C of all samples prepared is obtained using this criterion in this experiment.

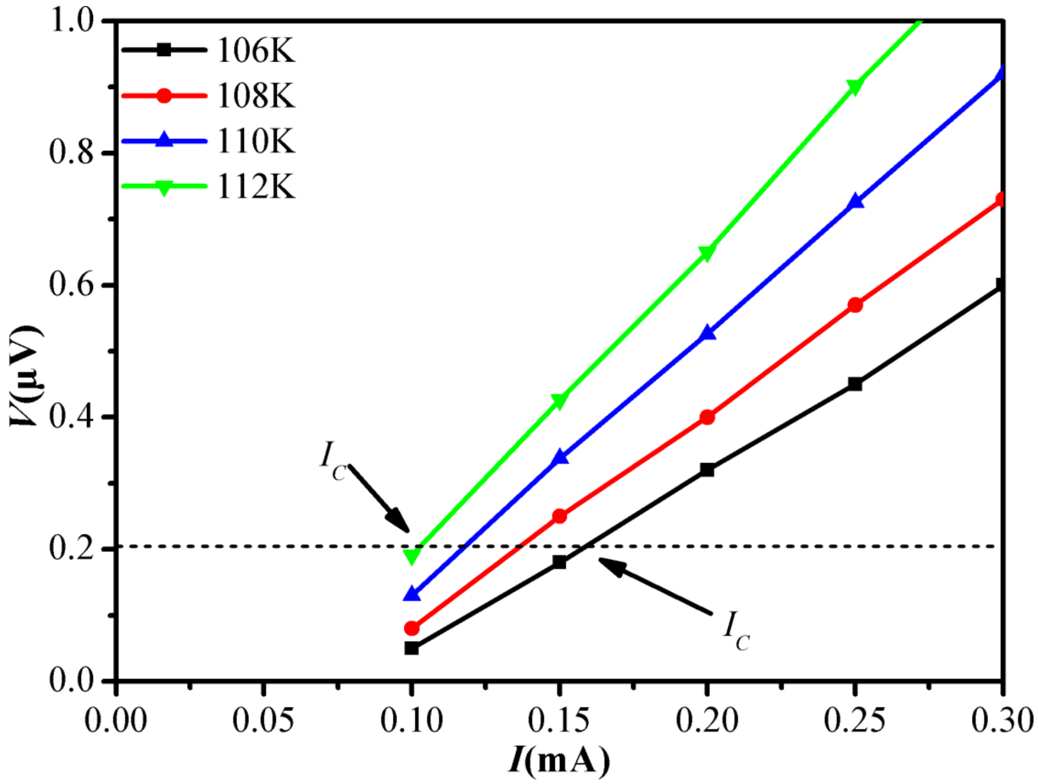

Figure 1. *I–V* curves of pure B(P)SCCO (A1) at 106, 108, 110, and 112 K.

Figure 2a,b show the relationship between J_C and the temperature of pure $^aMgB_2$ and $^aMgB_2$ doped with 0.5 wt% Y_2O_3:Sm^{3+}, Y_2O_3, Y_2O_3:Eu^{3+}, and Y_2O_3:Eu^{3+}+Ag. Figure 2c,d depict the relationship between J_C and the temperature of pure $^bMgB_2$ and $^bMgB_2$ doped with 0.8 wt% Y_2O_3:Sm^{3+}, Y_2O_3, Y_2O_3:Eu^{3+}, and Y_2O_3:Eu^{3+}+Ag. Figure 2e,f demonstrate the relationship between J_C and the temperature of pure $^cMgB_2$ and $^cMgB_2$ doped with 1.2 wt% Y_2O_3:Sm^{3+}, Y_2O_3, Y_2O_3:Eu^{3+}, and Y_2O_3:Eu^{3+}+Ag. The J_C of $^aMgB_2$, $^bMgB_2$, and $^cMgB_2$ are 8.9×10^4, 7.8×10^4, and 7.2×10^4 A/cm^2 at 20 K. As observed, the J_C of pure MgB_2 and doped samples decreases with the increase in temperature, which is consistent with the results of [28,47,48]. The J_C of pure MgB_2 is comparable to references [49,50]. The J_C decreases slowly when the temperature is lower, and the decreasing rate increases with the rise in temperature. The doping of Y_2O_3:Eu^{3+} and Y_2O_3:Eu^{3+}+Ag luminescent inhomogeneous phases increases the J_C. The $^cMgB_2$ series samples with the smallest particle size have a higher dopant content, and the most increases in J_C. At T = 34 K, the J_C of Y_2O_3:Eu^{3+} and Y_2O_3:Eu^{3+}+Ag doped samples increases by 32% and 38% compared with purely that of $^cMgB_2$, respectively. The J_C of non-luminescent dopant-doped MgB_2 samples first reduces to a minimum value, while the luminescent inhomogeneous phase-doped samples can have the J_C at a higher temperature. For example, the J_C of pure $^cMgB_2$ reduces to a minimum value at 36.8 K, and the J_C of 1.2 wt% Y_2O_3:Sm^{3+} and Y_2O_3 doped samples reduces to a minimum value at 35.8 and 35.6 K, while the J_C of 1.2 wt% Y_2O_3:Eu^{3+} and Y_2O_3:Eu^{3+}+Ag doped samples decreases to a minimum value at 37.8 and 38 K, respectively.

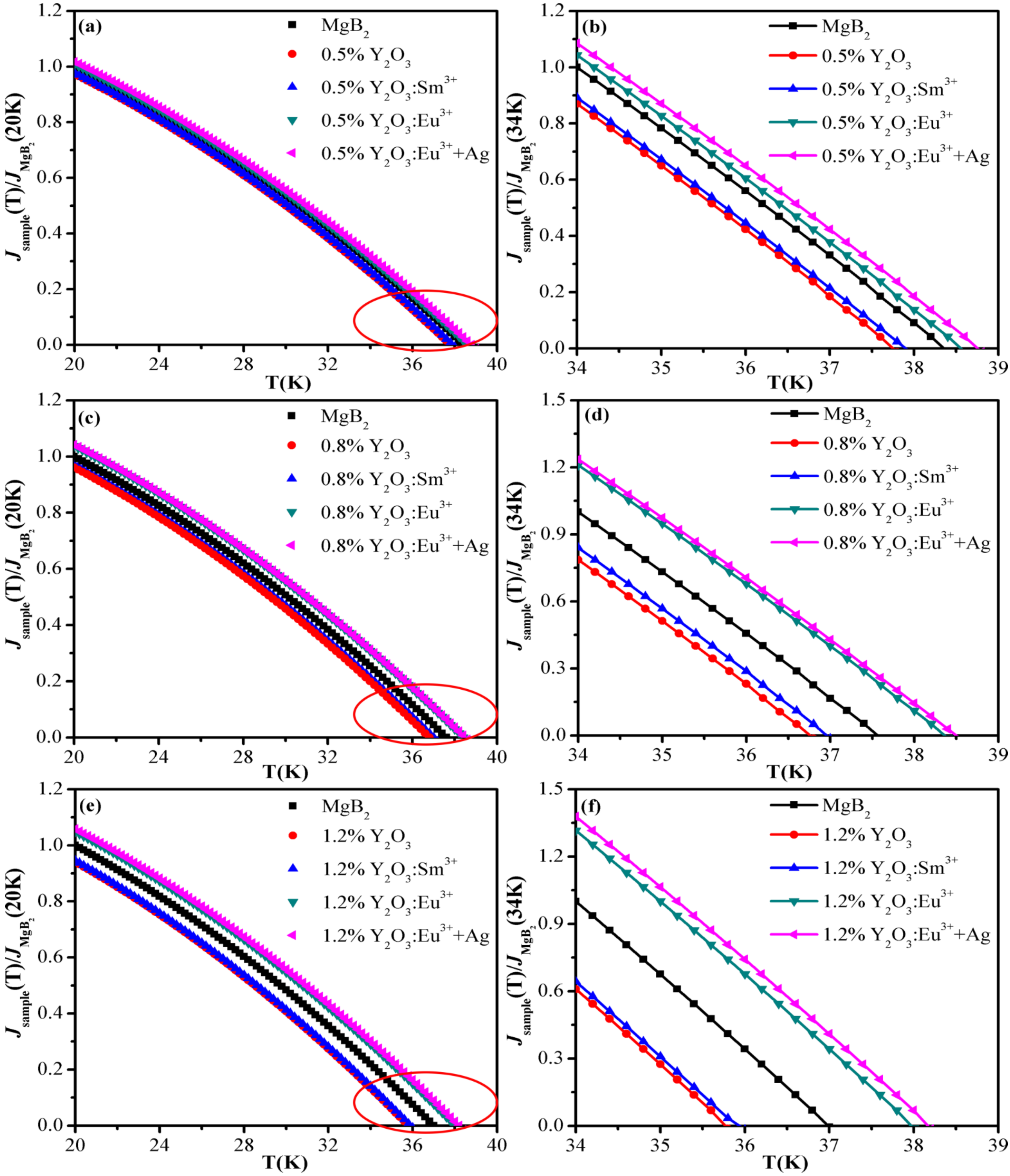

Figure 2. The relationship between J_C and temperature of pure MgB_2 and doping MgB_2 samples. (**a**,**b**) The relationship between J_C and temperature of pure $^{a}MgB_2$ and $^{a}MgB_2$ doped with 0.5 wt% Y_2O_3:Sm^{3+}, Y_2O_3, Y_2O_3:Eu^{3+}, and Y_2O_3:Eu^{3+}+Ag. (**c**,**d**) The relationship between J_C and temperature of pure $^{b}MgB_2$ and $^{b}MgB_2$ doped with 0.8 wt% Y_2O_3:Sm^{3+}, Y_2O_3, Y_2O_3:Eu^{3+}, and Y_2O_3:Eu^{3+}+Ag. (**e**,**f**) The relationship between J_C and temperature of pure $^{c}MgB_2$ and $^{c}MgB_2$ doped with 1.2 wt% Y_2O_3:Sm^{3+}, Y_2O_3, Y_2O_3:Eu^{3+}, and Y_2O_3:Eu^{3+}+Ag. (**b**,**d**,**f**) are partial enlarged images.

Figure 3a,b represent the relationship between J_C and temperature of pure B(P)SCCO (A1) and B(P)SCCO doped with 0.2 wt% $Y_2O_3:Sm^{3+}$ (A2), Y_2O_3 (A3), $Y_2O_3:Eu^{3+}$ (A4), $Y_2O_3:Eu^{3+}$+Ag (A5), and 0.3 wt% $Y_2O_3:Eu^{3+}$+Ag (A6). Figure 3c,d depict the relationship between J_C and temperature of pure B(P)SCCO (B1) and 0.2 wt% $Y_2O_3:Sm^{3+}$ (B2), Y_2O_3 (B3), $Y_2O_3:Eu^{3+}$ (B4), $Y_2O_3:Eu^{3+}$+Ag (B5), and 0.3 wt% $Y_2O_3:Eu^{3+}$+Ag (B6) doped samples. Figure 3e,f demonstrate the relationship between J_C and temperature of pure B(P)SCCO (C1) and B(P)SCCO doped with 0.3 wt% $Y_2O_3:Sm^{3+}$ (C2), 0.3 wt% Y_2O_3 (C3), 0.3 wt% $Y_2O_3:Eu^{3+}$ (C4), 0.3 wt% $Y_2O_3:Eu^{3+}$+Ag (C5), 0.4 wt% $Y_2O_3:Eu^{3+}$ (C6), and 0.4 wt% $Y_2O_3:Eu^{3+}$+Ag (C7). The J_C of B(P)SCCO (A1), B(P)SCCO (B1), and B(P)SCCO (C1) are 103, 70, and 54 A/cm^2 at 90 K. The figures show that the J_C of all samples decreases with the increase in temperature, which is consistent with [51,52]. The J_C of all samples decreases rapidly at lower temperature and slows down at higher temperature. This finding is completely contrary to the results observed for the conventional superconductor MgB_2. The J_C of pure B(P)SCCO is comparable to that of references [52–54]. $Y_2O_3:Eu^{3+}$ and $Y_2O_3:Eu^{3+}$+Ag luminescent inhomogeneous phase doping increases the J_C of B(P)SCCO, and the J_C of C-series samples with the smallest particle size increases the most. At T = 90 K, the J_C of $Y_2O_3:Eu^{3+}$ and $Y_2O_3:Eu^{3+}$+Ag luminescent inhomogeneous phase-doped samples increases by 80% and 95% compared with that of pure B(P)SCCO. Moreover, the J_C of luminescent inhomogeneous phase-doped samples decreases to a minimum value at higher temperature, while the J_C of non-luminescent dopant-doped samples decreases to a minimum value at lower temperature. For example, for C-series samples, the J_C of pure B(P)SCCO (C1) reduces to a minimum value at 107.5 K, and the J_C of 0.3 wt% $Y_2O_3:Sm^{3+}$ (C2), Y_2O_3 (C3) doped samples reduces to a minimum value at 106.5 and 106 K, respectively. While the J_C of 0.3 wt% $Y_2O_3:Eu^{3+}$ (C4), 0.3 wt% $Y_2O_3:Eu^{3+}$+Ag (C5), 0.4 wt% $Y_2O_3:Eu^{3+}$ (C6), and 0.4 wt% $Y_2O_3:Eu^{3+}$+Ag (C7) doped samples decreases to a minimum value at 110, 112, 112, and 113.5 K, respectively.

Figure 4 depicts the DC magnetization data of pure $^cMgB_2$ and $^cMgB_2$ doped with 1.2 wt% Y_2O_3, $Y_2O_3:Eu^{3+}$, and $Y_2O_3:Eu^{3+}$+Ag. Magnetization measurement shows that prepared samples have diamagnetism at a lower temperature. The diamagnetism of the superconductor can be represented by a Meissner effect, which is usually described in the literature by the relationship between the Meissner effect and temperature [46,55,56]. Therefore, we also showed the relationship between the Meissner effect and the temperature, as shown in Figure 4. The Y-axis is the percentage of the Meissner effect, indicating the strength of the Meissner effect (that is, the strength of the diamagnetism of the sample), and the X-axis is the temperature. The Meissner effect weakens and eventually disappears with the increase in temperature. The Meissner effect disappears at 36 K for pure $^cMgB_2$ sample, and it disappears at 34.6 K for the $^cMgB_2$ doped with non-luminescent dopant Y_2O_3. Meanwhile, the Meissner effect of $Y_2O_3:Eu^{3+}$ and $Y_2O_3:Eu^{3+}$+Ag luminescent inhomogeneous phase-doped $^cMgB_2$ samples disappears when temperature is higher than 36.8 and 37 K, respectively.

Figure 5 shows the DC magnetization data of pure B(P)SCCO (C1) and B(P)SCCO doped with 0.3 wt% Y_2O_3 (C3), $Y_2O_3:Eu^{3+}$ (C4), and $Y_2O_3:Eu^{3+}$+Ag (C5). Meissner effect is observed in all Bi(Pb)SrCaCuO samples by DC magnetization data, and the Meissner effect weakens and eventually disappears with the increase in temperature, which is consistent with the results of references [57–59]. The Meissner effect of pure B(P)SCCO disappears when the temperature is higher than 100 K, and that of B(P)SCCO doped with non-luminescent dopant Y_2O_3 disappears when the temperature is higher than 97 K. Meanwhile, the Meissner effect of $Y_2O_3:Eu^{3+}$ and $Y_2O_3:Eu^{3+}$+Ag luminescent inhomogeneous phase-doped samples disappears when the temperature is higher than 102 and 104 K, respectively.

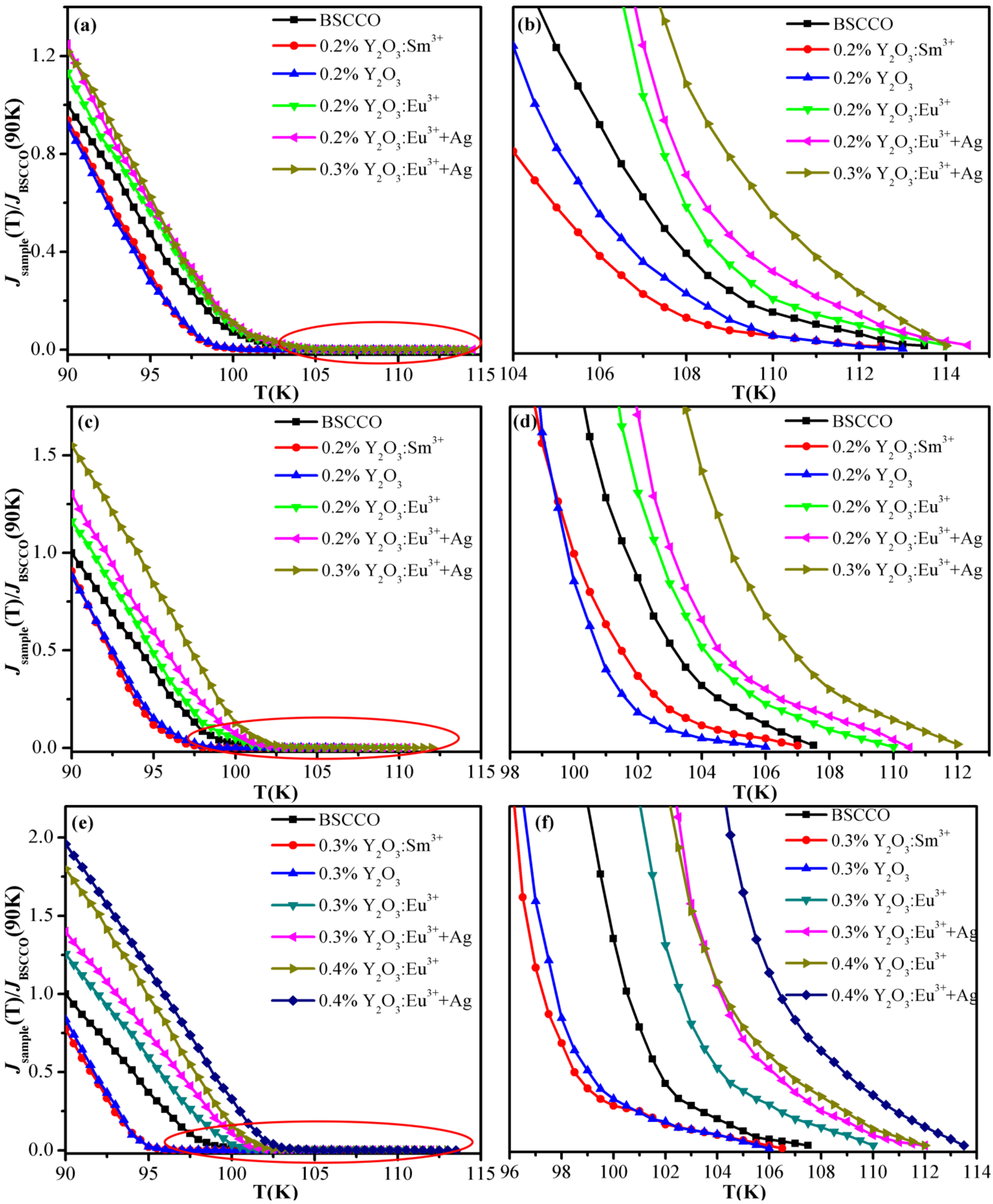

Figure 3. The relationship between J_C and temperature of pure B(P)SCCO and doping B(P)SCCO samples. (**a**,**b**) The relationship between J_C and temperature of pure B(P)SCCO (A1) and B(P)SCCO doped with 0.2 wt% Y_2O_3:Sm^{3+} (A2), Y_2O_3 (A3), Y_2O_3:Eu^{3+} (A4), Y_2O_3:Eu^{3+}+Ag (A5), and 0.3 wt% Y_2O_3:Eu^{3+}+Ag (A6). (**c**,**d**) The relationship between J_C and temperature of pure B(P)SCCO (B1) and 0.2 wt% Y_2O_3:Sm^{3+} (B2), Y_2O_3 (B3), Y_2O_3:Eu^{3+} (B4), Y_2O_3:Eu^{3+}+Ag (B5), and 0.3 wt% Y_2O_3:Eu^{3+}+Ag (B6) doped samples. (**e**,**f**) The relationship between J_C and temperature of pure B(P)SCCO (C1) and B(P)SCCO doped with 0.3 wt% Y_2O_3:Sm^{3+} (C2), Y_2O_3 (C3), Y_2O_3:Eu^{3+} (C4), Y_2O_3:Eu^{3+}+Ag (C5), 0.4 wt% Y_2O_3:Eu^{3+} (C6), and 0.4 wt% Y_2O_3:Eu^{3+}+Ag (C7). (**b**,**d**,**f**) are partial enlarged images.

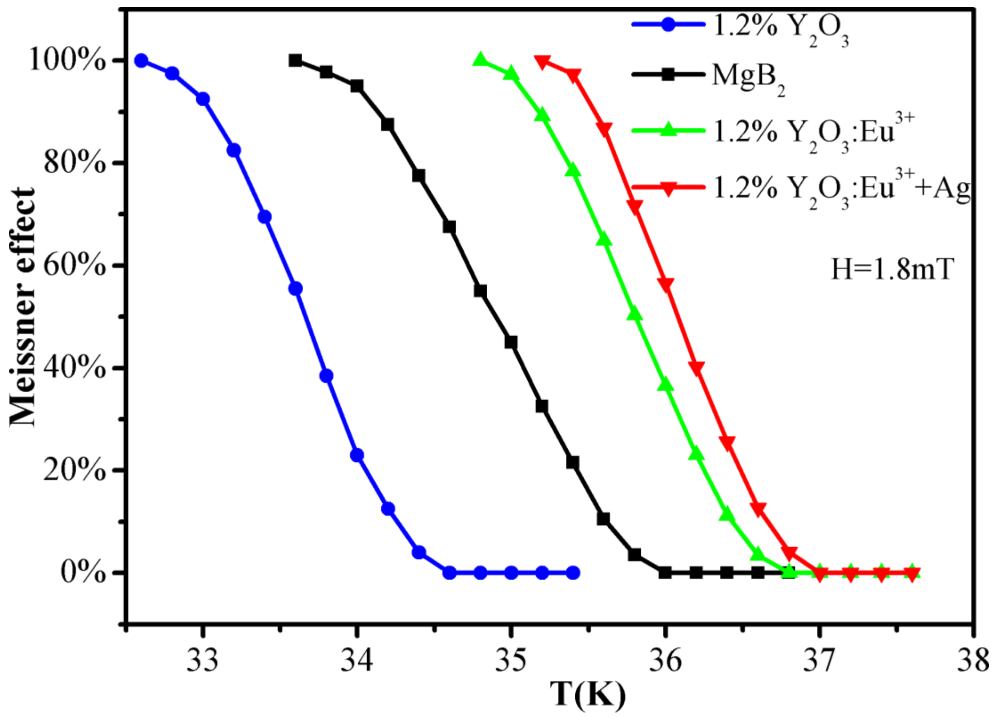

Figure 4. DC magnetization data of pure $^{c}MgB_2$ and $^{c}MgB_2$ doped with 1.2 wt% Y_2O_3, $Y_2O_3:Eu^{3+}$, and $Y_2O_3:Eu^{3+}$+Ag.

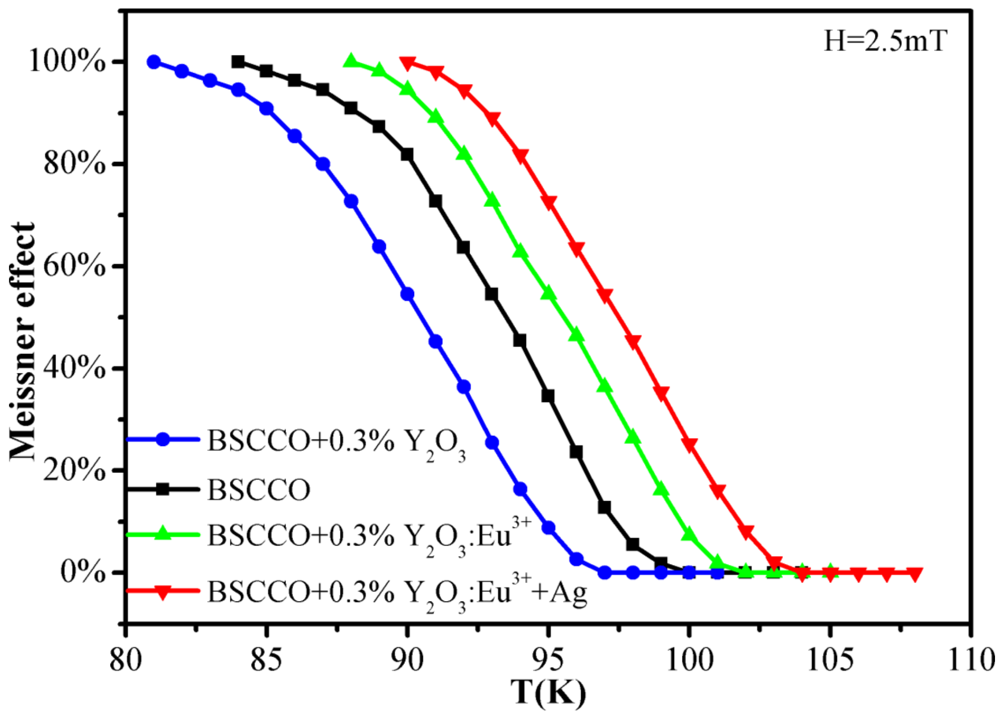

Figure 5. DC magnetization data of pure B(P)SCCO (C1) and B(P)SCCO doped with 0.3 wt% Y_2O_3 (C3), $Y_2O_3:Eu^{3+}$ (C4), and $Y_2O_3:Eu^{3+}$+Ag (C5).

In conventional MgB_2 and high-temperature copper oxide Bi(Pb)SrCaCuO superconductors, the sample doped with non-luminescent dopants has a Meissner effect at lower temperatures, while the Meissner effect is found in samples doped with a luminescent inhomogeneous phase at a higher temperature. Therefore, the superconductivity is enhanced by the doping of the luminescent inhomogeneous phase.

4. Conclusions

In this study, the *I*–*V* curves of Bi(Pb)SrCaCuO and MgB_2 smart meta-superconductor are measured by a four-probe method, the transport critical current density J_C is obtained and the changes in J_C are explored, the Meissner effect is also studied by DC magnetization measurement; the conclusions are as follows:

1. Y_2O_3:Eu^{3+}+Ag luminescent inhomogeneous phase doping increases the J_C of $^cMgB_2$ by 38% (T = 34 K), while the J_C of non-luminescent dopant-doped samples decreases. The J_C of pure $^cMgB_2$ decreases to a minimum value at 36.8 K, and the J_C of Y_2O_3:Eu^{3+} and Y_2O_3:Eu^{3+}+Ag-doped samples decreases to a minimum value at 37.8 and 38 K, respectively. Meanwhile, the J_C of Y_2O_3:Sm^{3+} and Y_2O_3-doped samples reduces to a minimum value at 35.8 and 35.6 K. The Meissner effect disappears at 36 K for pure $^cMgB_2$ sample, and it disappears at 36.8 and 37 K for Y_2O_3:Eu^{3+} and Y_2O_3:Eu^{3+}+Ag luminescent inhomogeneous phase-doped samples. Meanwhile, the Meissner effect disappears at 34.6 K for Y_2O_3 non-luminescent dopant-doped sample.
2. Y_2O_3:Eu^{3+}+Ag luminescent inhomogeneous phase doping increases the J_C of Bi(Pb)SrCaCuO by 95% (T = 90 K), the J_C of non-luminescent dopants doped samples decreases. The J_C of pure Bi(Pb)SrCaCuO (C1) decreases to a minimum value at 107.5 K. The J_C of Y_2O_3:Eu^{3+} and Y_2O_3:Eu^{3+}+Ag-doped samples decreases to a minimum value at 112 and 113.5 K, respectively. Meanwhile, the J_C of Y_2O_3:Sm^{3+} and Y_2O_3-doped samples reduces to a minimum value at 106.5 and 106 K. The Meissner effect of pure B(P)SCCO (C1) disappears when the temperature is higher than 100 K. The Meissner effect of Y_2O_3:Eu^{3+} and Y_2O_3:Eu^{3+}+Ag luminescent inhomogeneous phase-doped samples disappears when the temperature is higher than 102 and 104 K, while that of the Y_2O_3-doped sample disappears when the temperature is higher than 97 K.
3. The T_C and J_C of smart meta-superconductor MgB_2 and Bi(Pb)SrCaCuO increase simultaneously. The J_C of luminescent inhomogeneous phase-doped samples decreases to a minimum value at a higher temperature. A smart meta-superconductor has the Meissner effect at higher temperatures. All these findings indicate that the improvement in superconducting performance through a smart meta-superconductor is applicable to conventional and copper oxide high-temperature superconductors.

Author Contributions: Conceptualization, X.Z.; methodology, X.Z. and H.C.; software, H.C. and Y.Q.; validation, X.Z., H.C. and Y.Q.; formal analysis, X.Z., H.C., Y.L., Y.Q., M.W. and H.Z.; investigation, H.C., Y.L., Y.Q., M.W. and H.Z.; resources, X.Z.; data curation, H.C., Y.L., Y.Q., M.W. and H.Z.; writing—original draft preparation, H.C.; writing—review and editing, X.Z. and H.C.; visualization, X.Z. and H.C.; supervision, X.Z.; project administration, X.Z.; funding acquisition, X.Z. All authors have read and agreed to the published version of the manuscript.

Funding: This research was funded by the National Natural Science Foundation of China for Distinguished Young Scholar, grant number 50025207.

Institutional Review Board Statement: Not applicable.

Informed Consent Statement: Not applicable.

Data Availability Statement: The data presented in this study are available on request from the corresponding author.

Conflicts of Interest: The authors declare no conflict of interest. The funders had no role in the design of the study; in the collection, analyses, or interpretation of data; in the writing of the manuscript, or in the decision to publish the results.

References

1. Qiu, D.; Gong, C.; Wang, S.; Zhang, M.; Yang, C.; Wang, X.; Xiong, J. Recent Advances in 2D Superconductors. *Adv. Mater.* **2021**, *33*, e2006124. [CrossRef] [PubMed]
2. Gui, X.; Lv, B.; Xie, W.W. Chemistry in Superconductors. *Chem. Rev.* **2021**, *121*, 2966–2991. [CrossRef] [PubMed]
3. Bardeen, J.; Cooper, L.N.; Schrieffer, J.R. Theory of Superconductivity. *Phys. Rev.* **1957**, *108*, 1175–1204. [CrossRef]

4. Bardeen, J. Theory of the Meissner Effect in Superconductors. *Phys. Rev.* **1955**, *97*, 1724–1725. [CrossRef]
5. Chung, D.Y. The Basic Cause of Superconductivity. *J. Mod. Phys.* **2015**, *6*, 26–36. [CrossRef]
6. Fossheim, K.; Sudbø, A. What is Superconductivity? A Brief Overview. In *Superconductivity: Physics and Applications*; John Wiley & Sons Ltd.: Chichester, UK, 2004; pp. 1–26. [CrossRef]
7. Buckel, W.; Kleiner, R. Fundamental Properties of Superconductors. In *Superconductivity: Fundamentals and Applications*, 2nd ed.; Wiley-VCH, Verlag GmbH & Co. KgaA: Weinheim, Germany, 2004; pp. 11–71. [CrossRef]
8. Sunwong, P.; Higgins, J.S.; Tsui, Y.; Raine, M.J.; Hampshire, D.P. The critical current density of grain boundary channels in polycrystalline HTS and LTS superconductors in magnetic fields. *Supercond. Sci. Technol.* **2013**, *26*, 095006. [CrossRef]
9. Pautrat, A.; Simon, C.; Scola, J.; Goupil, C.; Ruyter, A.; Ammor, L.; Thopart, P.; Plessis, D. On voltage-current characteristics and critical current in Bi-2212. *Eur. Phys. J. B* **2005**, *43*, 39–45. [CrossRef]
10. Nappi, C.; Camerlingo, C.; Enrico, E.; Bellingeri, E.; Braccini, V.; Ferdeghini, C.; Sarnelli, E. Current Induced Resistive State in Fe(Se,Te) Superconducting Nanostrips. *Sci. Rep.* **2017**, *7*, 4115. [CrossRef]
11. Montemurro, D.; Stornaiuolo, D.; Massarotti, D.; Ercolani, D.; Sorba, L.; Beltram, F.; Tafuri, F.; Roddaro, S. Suspended InAs nanowire Josephson junctions assembled via dielectrophoresis. *Nanotechnology* **2015**, *26*, 385302. [CrossRef]
12. Rakshit, D.; Sk, T.; Das, P.; Haldar, S.; Ghosh, A.K. Exponential reduction in critical current density in $Eu_{1\text{-}x}Ce_xBa_2Cu_3O_{7\text{-}\delta}$ superconductors near critical temperature. *Phys. C Supercond.* **2021**, *588*, 1353909. [CrossRef]
13. Tampieri, A.; Fiorani, D.; Sparvieri, N.; Rinaldi, S.; Celotti, G.; Bartolucci, R. Granular and intergranular properties of hot pressed BSCCO (2223) superconductors. *J. Mater. Sci. Mater. Electron.* **1999**, *34*, 6177–6182. [CrossRef]
14. Cava, R.J.; Zandbergen, H.W.; Inumaru, K. The substitutional chemistry of MgB_2. *Phys. C Supercond.* **2003**, *385*, 8–15. [CrossRef]
15. Pogrebnyakov, A.V.; Xi, X.X.; Redwing, J.M.; Vaithyanathan, V.; Schlom, D.G.; Soukiassian, A.; Mi, S.B.; Jia, C.L.; Giencke, J.E.; Eom, C.B.; et al. Properties of MgB_2 thin films with carbon doping. *Appl. Phys. Lett.* **2004**, *85*, 2017–2019. [CrossRef]
16. Zhao, Y.G.; Zhang, X.P.; Qiao, P.T.; Zhang, H.T.; Jia, S.L.; Cao, B.S.; Zhu, M.H.; Han, Z.H.; Wang, X.L.; Gu, B.L. Effect of Li doping on structure and superconducting transition temperature of $Mg_{1-x}Li_xB_2$. *Phys. C Supercond.* **2001**, *361*, 91–94. [CrossRef]
17. Zhigadlo, N.D.; Petrashko, V.V.; Semenenko, Y.A.; Panagopoulos, C.; Cooper, J.R.; Salje, E.K.H. The effects of Cs doping, heat treatments on the phase formation and superconducting properties of (Bi,Pb)–Sr–Ca–Cu–O ceramics. *Phys. C Supercond.* **1998**, *299*, 327–337. [CrossRef]
18. Yavuz, Ş.; Bilgili, Ö.; Kocabaş, K. Effects of superconducting parameters of SnO_2 nanoparticles addition on (Bi, Pb)-2223 phase. *J. Mater. Sci. Mater. Electron.* **2016**, *27*, 4526–4533. [CrossRef]
19. Jia, Z.Y.; Tang, H.; Yang, Z.Q.; Xing, Y.T.; Wang, Y.Z.; Qiao, G.W. Effects of nano-ZrO_2 particles on the superconductivity of Pb-doped BSCCO. *Phys. C Supercond.* **2000**, *337*, 130–132. [CrossRef]
20. Drozdov, A.P.; Eremets, M.I.; Troyan, I.A.; Ksenofontov, V.; Shylin, S.I. Conventional superconductivity at 203 kelvin at high pressures in the sulfur hydride system. *Nature* **2015**, *525*, 73–76. [CrossRef]
21. Drozdov, A.P.; Kong, P.P.; Minkov, V.S.; Besedin, S.P.; Kuzovnikov, M.A.; Mozaffari, S.; Balicas, L.; Balakirev, F.F.; Graf, D.E.; Prakapenka, V.B.; et al. Superconductivity at 250 K in lanthanum hydride under high pressures. *Nature* **2019**, *569*, 528–531. [CrossRef]
22. Snider, E.; Dasenbrock-Gammon, N.; McBride, R.; Debessai, M.; Vindana, H.; Vencatasamy, K.; Lawler, K.V.; Salamat, A.; Dias, R.P. Room-temperature superconductivity in a carbonaceous sulfur hydride. *Nature* **2020**, *586*, 373–377. [CrossRef]
23. Tang, S.P.; Wang, D.L.; Zhang, X.P.; Zhang, Q.J.; Li, C.; Ma, Y.W.; Oguro, H.; Awaji, S.; Watanabe, K. Improved Transport J_C in MgB_2 Tapes by Graphene Doping. *J. Supercond. Nov. Magn.* **2014**, *27*, 2699–2705. [CrossRef]
24. Yang, Y.; Sumption, M.D.; Rindfleisch, M.; Tomsic, M.; Collings, E.W. Enhanced higher temperature irreversibility field and critical current density in MgB_2 wires with Dy_2O_3 additions. *Supercond. Sci. Technol.* **2021**, *34*, 025010. [CrossRef]
25. Annabi, M.; M'Chirgui, A.; Ben Azzouz, F.; Zouaoui, M.; Ben Salem, M. Addition of nanometer Al_2O_3 during the final processing of (Bi,Pb)-2223 superconductors. *Phys. C Supercond.* **2004**, *405*, 25–33. [CrossRef]
26. Hua, L.; Yoo, J.; Ko, J.; Kim, H.; Chung, H.; Qiao, G. Microstructure and phase evolution of ultrafine MgO doped Bi-2223/Ag tapes. *Phys. C Supercond.* **1997**, *291*, 149–154. [CrossRef]
27. Guo, Y.C.; Tanaka, Y.; Kuroda, T.; Dou, S.X.; Yang, Z.Q. Addition of nanometer SiC in the silver-sheathed Bi2223 superconducting tapes. *Phys. C Supercond.* **1999**, *311*, 65–74. [CrossRef]
28. Ahmad, I.; Sarangi, S.N.; Sarun, P.M. Enhanced critical current density and flux pinning of anthracene doped magnesium diboride superconductor. *J. Alloys Compd.* **2021**, *884*, 160999. [CrossRef]
29. Abbasi, H.; Taghipour, J.; Sedghi, H. Superconducting and transport properties of (Bi–Pb)–Sr–Ca–Cu–O with Cr_2O_3 additions. *J. Alloys Compd.* **2010**, *494*, 305–308. [CrossRef]
30. Abou-Aly, A.I.; Gawad, M.M.H.A.; Awad, R.; G-Eldeen, I. Improving the Physical Properties of (Bi,Pb)-2223 Phase by SnO_2 Nano-particles Addition. *J. Supercond. Nov. Magn.* **2011**, *24*, 2077–2084. [CrossRef]
31. Aftabi, A.; Mozaffari, M. Fluctuation induced conductivity and pseudogap state studies of $Bi_{1.6}Pb_{0.4}Sr_2Ca_2Cu_3O_{10+\delta}$ superconductor added with ZnO nanoparticles. *Sci. Rep.* **2021**, *11*, 4341. [CrossRef]
32. Zhao, X.P. Bottom-up fabrication methods of optical metamaterials. *J. Mater. Chem.* **2012**, *22*, 9439–9449. [CrossRef]
33. Liu, H.; Zhao, X.P.; Yang, Y.; Li, Q.W.; Lv, J. Fabrication of Infrared Left-Handed Metamaterials via Double Template-Assisted Electrochemical Deposition. *Adv. Mater.* **2008**, *20*, 2050–2054. [CrossRef]
34. Smolyaninov, I.I.; Smolyaninova, V.N. Metamaterial superconductors. *Phys. Rev. B* **2015**, *91*, 094501. [CrossRef]

35. Smolyaninov, I.I.; Smolyaninova, V.N. Is There a Metamaterial Route to High Temperature Superconductivity? *Adv. Condens. Matter Phys.* **2014**, *2014*, 479635. [CrossRef]
36. Rosen, P.F.; Calvin, J.J.; Woodfield, B.F.; Smolyaninova, V.N.; Prestigiacomo, J.C.; Osofsky, M.S.; Smolyaninov, I.I. Normal state specific heat of a core-shell aluminum-alumina metamaterial composite with enhanced T_C. *Phys. Rev. B* **2021**, *103*, 024512. [CrossRef]
37. Zhang, Z.W.; Tao, S.; Chen, G.W.; Zhao, X.P. Improving the Critical Temperature of MgB_2 Superconducting Metamaterials Induced by Electroluminescence. *J. Supercond. Nov. Magn.* **2016**, *29*, 1159–1162. [CrossRef]
38. Tao, S.; Li, Y.B.; Chen, G.W.; Zhao, X.P. Critical Temperature of Smart Meta-superconducting MgB_2. *J. Supercond. Nov. Magn.* **2017**, *30*, 1405–1411. [CrossRef]
39. Li, Y.B.; Chen, H.G.; Qi, W.C.; Chen, G.W.; Zhao, X.P. Inhomogeneous Phase Effect of Smart Meta-Superconducting MgB_2. *J. Low Temp. Phys.* **2018**, *191*, 217–227. [CrossRef]
40. Chen, H.G.; Li, Y.B.; Chen, G.W.; Xu, L.X.; Zhao, X.P. The Effect of Inhomogeneous Phase on the Critical Temperature of Smart Meta-superconductor MgB_2. *J. Supercond. Nov. Magn.* **2018**, *31*, 3175–3182. [CrossRef]
41. Li, Y.B.; Chen, H.G.; Wang, M.Z.; Xu, L.X.; Zhao, X.P. Smart meta-superconductor MgB_2 constructed by the dopant phase of luminescent nanocomposite. *Sci. Rep.* **2019**, *9*, 14194. [CrossRef]
42. Chen, H.G.; Li, Y.B.; Wang, M.Z.; Han, G.Y.; Shi, M.; Zhao, X.P. Smart Metastructure Method for Increasing T_C of Bi(Pb)SrCaCuO High-Temperature Superconductors. *J. Supercond. Nov. Magn.* **2020**, *33*, 3015–3025. [CrossRef]
43. Chen, H.G.; Wang, M.Z.; Qi, Y.; Li, Y.B.; Zhao, X.P. Relationship between the T_C of Smart Meta-Superconductor Bi(Pb)SrCaCuO and Inhomogeneous Phase Content. *Nanomaterials* **2021**, *11*, 1061. [CrossRef] [PubMed]
44. Li, Y.B.; Han, G.Y.; Zou, H.Y.; Tang, L.; Chen, H.G.; Zhao, X.P. Reinforcing Increase of ΔT_C in MgB_2 Smart Meta-Superconductors by Adjusting the Concentration of Inhomogeneous Phases. *Materials* **2021**, *14*, 3066. [CrossRef] [PubMed]
45. Wang, M.Z.; Xu, L.X.; Chen, G.W.; Zhao, X.P. Topological luminophor Y_2O_3:Eu^{3+}+Ag with high electroluminescence performance. *ACS Appl. Mater. Interfaces* **2019**, *11*, 2328–2335. [CrossRef] [PubMed]
46. Sunshine, S.A.; Siegrist, T.; Schneemeyer, L.F.; Murphy, D.W.; Cava, R.J.; Batlogg, B.; van Dover, R.B.; Fleming, R.M.; Glarum, S.H.; Nakahara, S.; et al. Structure and physical properties of single crystals of the 84-K superconductor $Bi_{2.2}Sr_2Ca_{0.8}Cu_2O_{8+\delta}$. *Phys. Rev. B* **1988**, *38*, 893–896. [CrossRef] [PubMed]
47. Buzea, C.; Yamashita, T. Review of superconducting properties of MgB_2. *Supercond. Sci. Technol.* **2001**, *14*, R115–R146. [CrossRef]
48. Zhang, H.; Zhao, Y.; Zhang, Y. The Effects of Excess Mg Addition on the Superconductivity of MgB_2. *J. Supercond. Nov. Magn.* **2015**, *28*, 2711–2714. [CrossRef]
49. Arvapalli, S.S.; Miryala, M.; Jirsa, M.; Murakami, M. Size reduction of boron particles by high-power ultrasound for optimization of bulk MgB_2. *Supercond. Sci. Technol.* **2020**, *33*, 115009. [CrossRef]
50. Peng, J.M.; Cai, Q.; Cheng, F.; Ma, Z.Q.; Li, C.; Xin, Y.; Liu, Y.C. Enhancement of critical current density by a "MgB_2 -MgB_4 " reversible reaction in self-sintered ex-situ MgB_2 bulks. *J. Alloys Compd.* **2017**, *694*, 24–29. [CrossRef]
51. Karaca, I.; Celebi, S.; Varilci, A.; Malik, A.I. Effect of Ag_2O addition on the intergranular properties of the superconducting Bi-(Pb)-Sr-Ca-Cu-O system. *Supercond. Sci. Technol.* **2003**, *16*, 100–104. [CrossRef]
52. Shamsodini, M.; Salamati, H.; Shakeripour, H.; Sarsari, I.A.; Esferizi, M.F.; Nikmanesh, H. Effect of using two different starting materials (nitrates and carbonates) and a calcination processes on the grain boundary properties of a BSCCO superconductor. *Supercond. Sci. Technol.* **2019**, *32*, 075001. [CrossRef]
53. Manabe, T.; Tsunoda, T.; Kondo, W.; Shindo, Y.; Mizuta, S.; Kumagai, T. Preparation and Superconducting Properties of Bi-Pb-Sr-Ca-Cu-O Films (T_C = 106 K) by the Dipping-Pyrolysis Process. *Jpn. J. Appl. Phys.* **1992**, *31*, 1020–1025. [CrossRef]
54. Ghattas, A.; Annabi, M.; Zouaoui, M.; Azzouz, F.B.; Salem, M.B. Flux pinning by Al-based nano particles embedded in polycrystalline (Bi,Pb)-2223 superconductors. *Phys. C Supercond.* **2008**, *468*, 31–38. [CrossRef]
55. Nam, S.B. Magnetization of Superconducting Ba (Y, Nd, Sm, Gd, Dy, Er, Yb) CuO Systems. *Jpn. J. Appl. Phys.* **1987**, *26*, 1175. [CrossRef]
56. Schwenk, H.; Andres, K.; Wudl, F. Anisotropy of the lower critical field and meissner effect in $(TMTSF)_2ClO_4$ in the basal plane. *Solid State Commun.* **1984**, *49*, 723–726. [CrossRef]
57. Krishna, N.M.; Lingam, L.S.; Ghosh, P.K.; Shrivastava, K.N. Effect of current-loop sizes on the para-Meissner effect in superconductors. *Physica C Supercond* **1998**, *294*, 243–248. [CrossRef]
58. Posselt, H.; Muller, H.; Andres, K.; Saito, G. Reentrant Meissner effect in the organic conductor κ-$(BEDT\text{-}TTF)_2Cu[N(CN)_2]Cl$ under pressure. *Phys. Rev. B* **1994**, *49*, 15849–15852. [CrossRef]
59. Horiuchi, T.; Kawai, T.; Kawai, S.; Ogura, K. The trial of making Bi-Sr-Ca-Cu-M-O superconductors (M = Li, Na, K, Rb, Cs). *Ferroelectrics* **1990**, *109*, 351–356. [CrossRef]